HTML ABSTRACT + LINKS

Behavior of a movable electrode in piezo-response mode of an atomic force microscope

C. H. Xu,[a] C. H. Woo, and S. Q. Shi
Department of Mechanical Engineering, The Hong Kong Polytechnic University, Hunghom, Kowloon, Hong Kong, SAR China

Y. Wang
Department of Applied Physics, The Hong Kong Polytechnic University, Hunghom, Kowloon, Hong Kong, SAR China

(Received 5 February 2004; accepted 22 March 2004)

The objective of this work was to understand the effect of the movable electrode (the tip of an atomic force microscope) on a piezoelectric-induced (PEI) image. Local polarization is induced on a lead zirconate titanate (PZT) thin film using an atomic force microscope (AFM), by applying dc voltage between the movable electrode and the Pt bottom electrode. The polarized PZT film is then characterized by the AFM using a two-pass method, in which both the topography and PEI image are obtained. The surface morphology is recorded in the first pass under contact mode with a fixed setpoint. A PEI image is obtained in the second pass in piezo-response mode. In this mode, the sample surface is scanned by applying ac voltage between the AFM tip and the Pt bottom electrode at sample displacement. PEI images of various sample displacement, corresponding to different stress exerted by the tip on the sample surface, are obtained and analyzed using force–sample displacement curves. It is found that PEI images can be detected if the tip adheres to the sample. The asymmetry of the $A \cos \theta$ signal is improved as the force changes from repulsive to attractive. © *2004 American Institute of Physics.* [DOI: 10.1063/1.1739532]

I. INTRODUCTION

During the past decade, the scanning probe microscope (SPM) has quickly become an essential tool for materials research. Scanning tunneling microscopes (STMs) and atomic force microscopes (AFM) have been found to be useful in the study of domain structures in ferroelectric thin films,[1,2] their advantage being the ease in sample preparation, their nondestructive characterization, and their high spatial resolution. AFM has been used in piezo-responsive mode to detect piezoelectric vibrations in ferroelectric films.[3,4] For this, the AFM is operated in contact mode with ac voltage through the ferroelectric film applied between the conductive AFM tip and the bottom electrode. The signal, consisting of the dc and the first harmonic, is detected by a laser photodetector, and goes through a low pass filter. The dc signal through the low pass filter gives the surface topography. The first harmonic is blocked by the low pass filter, and goes through a lock-in amplifier and produces a piezoelectric-induced (PEI) image. Small ac voltage through the ferroelectric film induces local piezoelectric vibration, which can be detected by the AFM tip and forms the PEI image. The PEI image is recorded as an $A \cos \theta$ signal.[5] Here, A is the amplitude of the first harmonic signal, which provides information on the magnitude of the piezoelectric coefficient (d_{33}). θ is the shift in phase between the signal of ac voltage applied and the responding first harmonic,[4] which determines the direction of polarization.[5]

In contact mode, compressive force is usually exerted by the tip onto the surface of the sample during measurement, which may affect the d_{33} values of lead zirconate titanate (PZT) films.[6] Some authors have suggested using tips with high force constant (48 N/m)[7] to measure PEI images, and others have suggested low force constant tips (0.09 N/m)[8] to alleviate the problem.

Adsorption of water on the surface of a sample in a ambient atmosphere is another frequently encountered problem that may adversely affect the quality of an AFM image. Thus, N_2 gas[9] or a vacuum environment[10] is often used to obtain PEI images.

The topography and PEI image of the PZT thin film are separated by using a two-pass method in this article. The surface topography is obtained in contact mode in the first pass. The PEI image is measured with ac voltage between the AFM tip and the bottom electrode in the second pass. The topography and PEI image are alternately scanned line by line in the two-pass method. The force between the AFM tip and the sample in the second pass can be adjusted by the sample displacement to height ΔZ.

II. EXPERIMENTAL PROCEDURE

PZT thin films are prepared by conventional sol–gel and spin coating techniques. A SiO_2 film with a thickness of about 550 nm is deposited by thermal diffusion onto a 0.5 mm Si wafer. The bottom electrode, Pt (80 nm)/Ti (120 nm), is deposited by sputtering onto the SiO_2/Si wafer. The PZT solution is spin coated onto the Pt/Ti/SiO_2/Si substrate, followed by drying on a hotplate at 250 °C for 5 min to remove

[a]Electronic mail: mmcjxu@polyu.edu.hk

 © 2004 American Institute of Physics

Downloaded 18 Mar 2011 to 158.132.161.9. Redistribution subject to AIP license or copyright; see http://jap.aip.org/about/rights_and_permissions

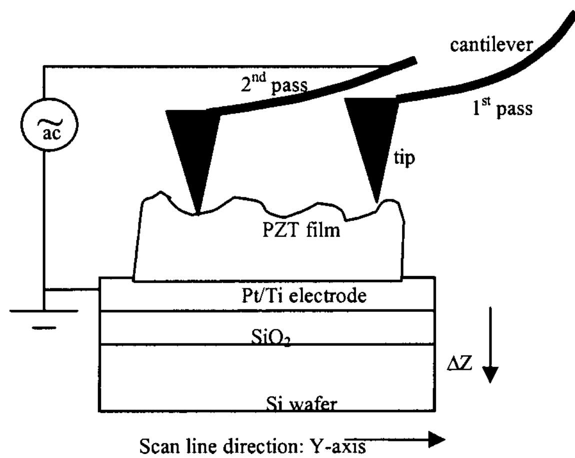

FIG. 1. Illustration of measuring topography and PEI image in the two-pass method: recording topography by contact mode in the first pass, then displacing sample ΔZ; performing PEI image by applying ac voltage between the tip and Pt bottom electrode at height ΔZ in the second pass.

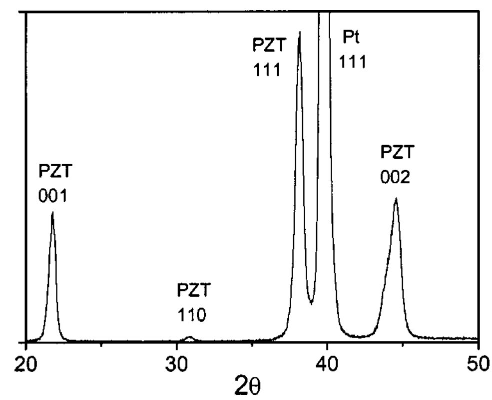

FIG. 2. X-ray diffraction spectra of the PZT film showing a pure perovskite phase with random orientation.

any organic matter in the solution. This process is repeated five times until the film grows to about 200 nm. The composition of PZT is $Pb_{1.1}(Zr_{0.53}Ti_{0.47})O_3$. The final thermal treatment is to crystallize the PZT by rapid thermal annealing (RTA) in oxygen. The annealing temperature is 600 °C at a ramp up rate of about 250 °C/min and an annealing time of 10 min. After annealing, the crystal structure of the PZT film is examined with a Philips PW3710 x-ray diffractometer using Cu $K\alpha$ x rays at 30 kV and 40 mA.

Local poling of the PZT film and detection of the PEI images are carried out on a SOLVER P47H atomic force microscope using a conductive W_2C-coated Si cantilever with force constant of 3 N/m, and an integrated tip with an apex curvature radius of about 35 nm. Dc voltages of +10 and −10 V are applied between the tip and the Pt bottom electrode, respectively. The surface topography and the PEI image are obtained in the two-pass method with a scan rate of 19 800 nm/s, as illustrated in Fig. 1. The surface topography is scanned in contact mode at a fixed setpoint in the first pass. In the second pass, the sample displaces ΔZ in the direction away from the tip and the PEI image is, then, obtained with a disabling feedback loop and ac voltage of 1 V at frequency of 200 kHz between the tip and the Pt electrode. The scan line directions in both passes are along the Y axis from 0 to 3.5 μm. ΔZ varies between 0 and 250 nm. The force between the tip and the sample surface is measured as a function of sample displacement ΔZ with or without applying 1 V ac voltage.

III. RESULTS

Compared with standard x-ray diffraction spectra, the x-ray diffraction spectra of the PZT film in Fig. 2 show a pure perovskite phase with random orientation.

The relationship between force and sample displacement is shown in Fig. 3. Figure 3(a) shows a curve of force and sample displacement measured without applying ac voltage. Positive and negative force represents repulsion and attraction between the tip and sample, respectively. From A→B→C′→C, the sample moves towards the tip; and from D→D′→E→F→A, the sample retreats from it. When the surface of the sample is far from the tip at A, the force is zero. At B, the tip starts to encounter attractive force due to the sample. When closer, repulsive force starts to develop from point C′, the strength of which increases as the contact increases along C′–C. At C, the sample starts to reverse the direction and a jump occurs from C to D. The

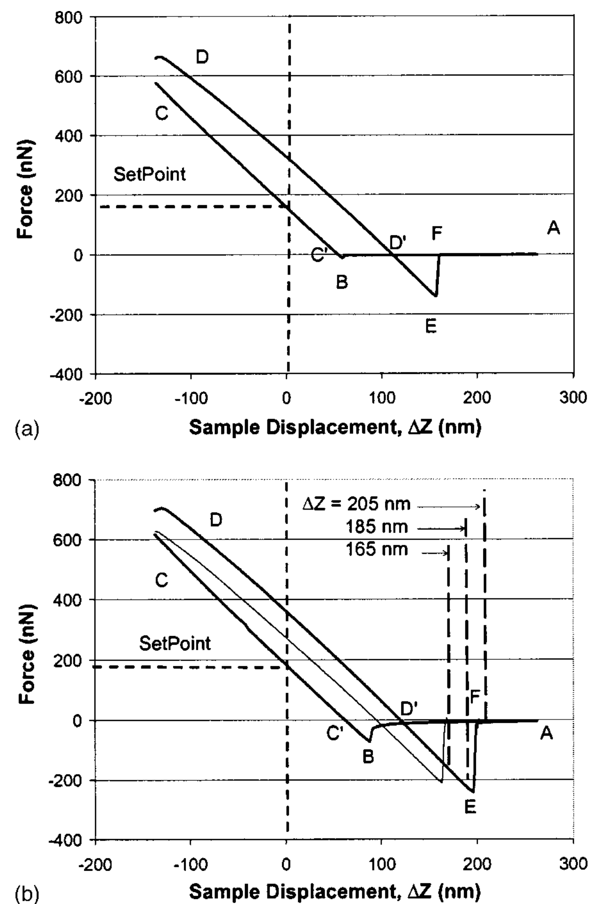

FIG. 3. Force–sample displacement curves measured (a) without ac voltage and (b) with 1 V ac voltage between the tip and the Pt electrode. The sample displaces towards the tip along curve A–B–C′–C and away from the tip along curve D–D′–E–F–A. Pull-off force at point E is related to separation of the tip from the sample. The curves with thin and thick solid lines stand for 0 and 200 nm stays of the tip at position C–D.

Downloaded 18 Mar 2011 to 158.132.161.9. Redistribution subject to AIP license or copyright; see http://jap.aip.org/about/rights_and_permissions

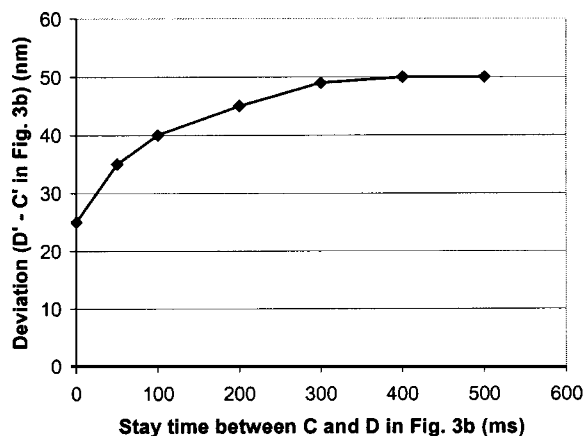

FIG. 4. Stay time at the position to change the direction of sample displacement vs deviation of point D′ from point C′ in Fig. 3(b).

repulsive force is reduced as the surface of the sample continues to retreat from the tip, and subsequently becomes attractive from point D′. The maximum attractive force on the sample upon retraction (point E), called pull-off force, is much larger than that when it approaches (point B). The curve jumped from E to F, when the tip and sample were disconnected.

Figure 3(b) shows the curve of force and sample displacement, which is obtained by applying 1 V ac voltage on the PZT film. Compared with Fig. 3(a), the ac voltage causes attractive force at a long distance (line A–B that deviates from 0 force) and increases the attractive force at point B and the pull-off force at point E.

The deviation of the D–D′ line from the C–C′ line in Fig. 3 cannot be explained properly so far. Possible reasons are the inelastic response of the tip–sample system, and the hysteresis and creep of the piezoelectric ceramics which are in the scanner to move the sample.[11,12] In the present experiment, we find that the intensity of the deviation also relates to the stay time between points C and D. Figure 4 shows the curve of the stay time between points C and D versus the deviation of point D′ from point C′ in Fig. 3(b). Deviation occurs even for a 0 ms stay. When the stay time changes from 0 to 300 ms, the deviation is almost double. The curves with thick solid lines in Fig. 3 were obtained with 200 ms stay between points C and D while the curve with the thin solid line in Fig. 3(b) is obtained with 0 ms stay. The stay time between points C and D also affects the pull-off force, as shown in the Fig. 3(b).

The topography and PEI images with the various sample displacement ΔZ are shown in Fig. 5. The scales beside the bar on the right of Fig. 5 show the signal contract. Figures 5(a) and 5(b) give the topography and the PEI image, respectively, at the setpoint ($\Delta Z=0$). Positively and negatively poled areas can be seen clearly in Fig. 5(b). PEI images at sample displacement ΔZ of 25, 45, and 65 and up to 165 nm are similar to that in Fig. 5(b). Figures 5(c) and 5(d) are PEI images at sample displacement heights of 185 and 205 nm, respectively. The PEI images are gradually lost along the scan line direction, the Y axis, with an increase in sample displacement. If the scan direction in the second pass were reversed, the dark line in Figs. 5(c) and 5(d) would also overturn, indicating that the PEI image disappears during scanning. The PEI image totally disappears at sample dis-

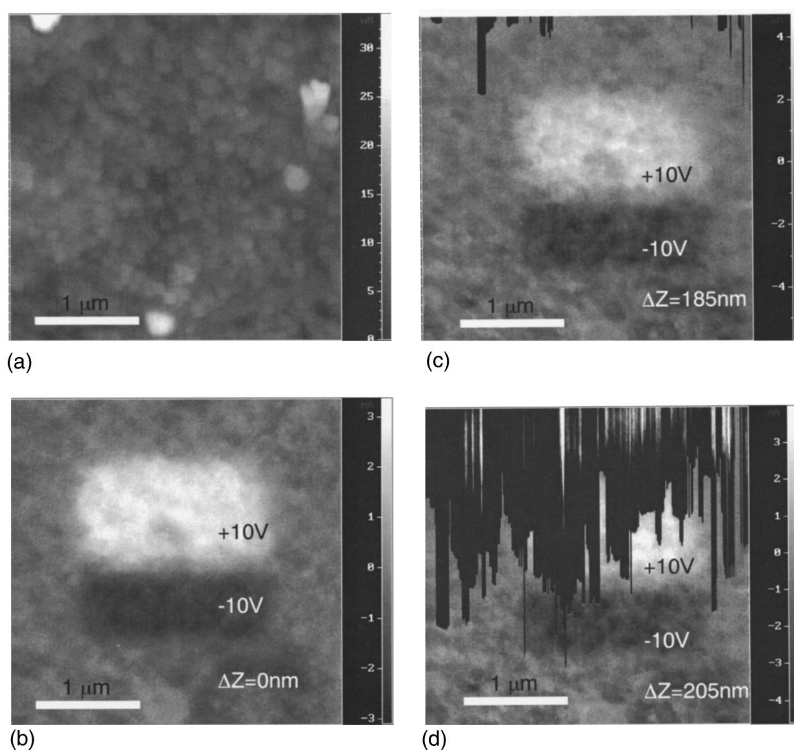

FIG. 5. Topography and PEI images at different sample displacement ΔZ: (a) topography, (b) PEI image at $\Delta Z=0$, (c) PEI image at $\Delta Z=185$ nm, and (d) PEI image at $\Delta Z=205$ nm. The scales beside the bar on the right of (a)–(d) show the signal contract.

Downloaded 18 Mar 2011 to 158.132.161.9. Redistribution subject to AIP license or copyright; see http://jap.aip.org/about/rights_and_permissions

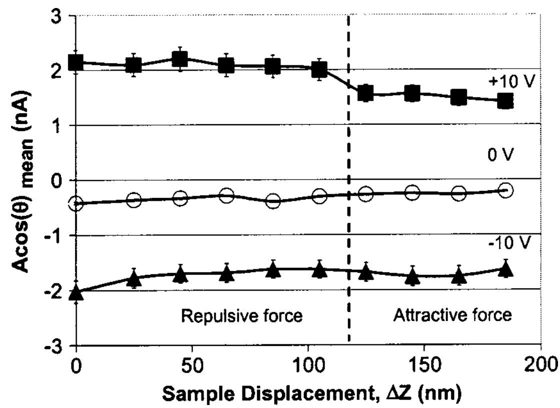

FIG. 6. Mean of the intensity of the $A \cos \theta$ signal at positive, negative and no-poling areas vs sample displacement, showing that $A \cos \theta$ signals are asymmetrical under repulsive force and nearly symmetrical under attractive force.

placement of more than 220 nm. The intensity of the $A \cos \theta$ signal at each scan point can be read from the PEI image. The mean of the intensity of $A \cos \theta$ on $+10$, -10, and 0 V areas are calculated using SOLVER P47H software, and is plotted according to sample displacement (0–185 nm) in Fig. 6.

IV. DISCUSSION

A. Effects of ac voltage on static and pull-off forces

The ac voltage increases the attractive force at long distances[5,13] and the pull-off force (Fig. 3). The static force F_{static} on a tip in noncontact mode [A–B line in Fig. 3(b)] can be caused by electric fields, according to

$$F_{\text{static}} = k_{\text{lever}} \times z_{\text{static}} = -\frac{\partial C}{2 \partial z}\left[(V_{\text{dc}} - V_C)^2 - \frac{V_{\text{ac}}^2}{2}\right], \qquad (1)$$

where z_{static} is the static displacement of a tip; C is the electric capacitance between the tip–cantilever system and the Pt bottom electrode; z is the distance between the tip and the Pt electrode; k_{lever} is the force constant of the cantilever (equal to 3 N/m); V_{dc} and V_{ac} are the dc (equal to 0) and ac (equal to 1) voltages applied on the tip, respectively; V_C is the difference in potential between the tip–cantilever system and the sample. From Eq. (1), the static force is always attractive, which is shown as the deviation in line A–B from the horizontal line in Fig. 3(b).

The force required to separate the tip and sample surfaces is known as pull-off force. The magnitude of the force depends on the area of contact and the nature of the attractive forces holding the surface together. These forces include van der Waals, capillary or electrostatic force.[14] For a nondeformable solid sample in ambient atmosphere, the pull-off force in Fig. 3(a) can be expressed as

$$F_{\text{pull off}} = F_{\text{van der Waals}} + F_{\text{capillary}}, \qquad (2)$$

where $F_{\text{van der Waals}}$ is the van der Waals force, which can be evaluated at point B in Fig. 3(a); $F_{\text{capillary}}$ is the capillary force due to the meniscus force exerted by a thin layer of water vapor adsorbed on the sample surface.[15] $F_{\text{pull off}}$ for AFM operation in ambient atmosphere can be typically by increased two orders of magnitude compared with liquid conditions,[14] suggesting $F_{\text{pull off}}$ is mainly dominated by $F_{\text{capillary}}$.

$F_{\text{pull off}}$ in Fig. 3(b) is larger than that in Fig. 3(a), which can be expressed as

$$F_{\text{pull off}} = F_{\text{van der Waals}} + F_{\text{capillary}} + F_{\text{static}}, \qquad (3)$$

F_{static} can be evaluated by Eq. (1). The attractive forces at point B in Figs. 3(a) and 3(b) are 3 and 64 nN, respectively, showing that 1 V ac voltage can cause an increase of 61 nN in static force. According to Eq. (3), $F_{\text{pull off}}$ in Fig. 3(b) can be evaluated from $F_{\text{pull off}}$ in Fig. 3(a) (137 nN) plus the force at point B in Fig. 3(b) (64 nN) as 200 nN, which is close to the value of 230 nN at point E in Fig. 3(b).

B. Effects of the movable electrode on the PEI image

From Fig. 5, the whole PEI image can be seen up to sample displacement of 165 nm. The PEI images can still be seen partially in Figs. 5(c) and 5(d) with an increase in sample displacement up to 205 nm. Sample displacement of 165, 185, and 205 nm is shown by dotted lines in Fig. 3(b). The stay time between points C and D in Fig. 3(b) can also affect $F_{\text{pull off}}$. The positions of $F_{\text{pull off}}$ in Fig. 3(b) at the curve with 0 ms stay (thin line) and at the curve with 200 ms stay (thick line) are at $\Delta Z = 161$ and 196 nm, respectively. Based on the scanning rate of 19 800 nm/s in the present experiment, the time to scan one line in the first pass is about 180 ms. In the other words, the difference in time between the topography and PEI image is 180 ms at the same position. Time is also needed for moving the tip from the end of the first pass to the beginning of the second pass. Part of the PEI image disappears at sample displacement of 185–205 nm [see Figs. 5(c) and 5(d)], which is close to the position ($\Delta Z = 196$ nm) of $F_{\text{pull off}}$ on the thick line curve. This implies that the interval of time between two passes may affect the critical value of sample displacement, at which time the PEI image disappears. From analysis of Fig. 3(b), the PEI image can be obtained if the tip touches the sample.

The $A \cos \theta$ signal in piezo-response mode during AFM measurement relates to the ac field-induced strain, d_{33} according to[5]

$$A \cos \theta = -\frac{\partial C / \partial z}{k_{\text{lever}}}(V_{\text{dc}} - V_C) V_{\text{ac}} \pm d_{33} V_{\text{ac}}. \qquad (4)$$

The electrically induced strain for piezoelectric materials is usually measured under compressive stress. From Fig. 6, the $A \cos \theta$ signal on the $+10$ V poling area is significantly larger that in the -10 V poling area under repulsive force. Similar asymmetry has been reported in the measurement of d_{33} on $SrBi_2Ta_2O_9$ thin film by AFM[7] and on PZT film with top and bottom electrodes by the traditional method.[16] This asymmetry was interpreted in terms of the effective clamping of some domains in preferential orientations leading to d_{33} offset[17] or in terms of residual stress between the substrate and the thin layers,[16] which results in the different movability of the non-180° domain wall at the positive and negative poling areas. When the repulsive force on the surface of the

Downloaded 18 Mar 2011 to 158.132.161.9. Redistribution subject to AIP license or copyright; see http://jap.aip.org/about/rights_and_permissions

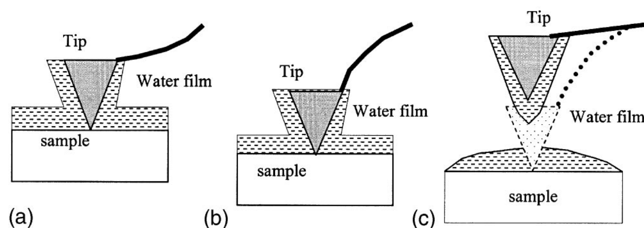

FIG. 7. Schematic of the tip position with sample displacement during the second pass: (a) repulsive force, (b) attractive force, and (c) water bridge broken during scanning.

sample is removed ($\Delta Z > 120\,\text{nm}$), the $A\cos\theta$ signals in the +10 V poling area are reduced about 22% and the asymmetry of $A\cos\theta$ signals is significantly reduced. If the 0 V curve in Fig. 6 is offset, the signal of external stress on the sample applied by the AFM tip significantly influences the $A\cos\theta$ asymmetry. External stress may result in the redistribution of residual stress in the film and change movement of non-180° domain walls.

Generally, $A\cos\theta$ signals in both poling areas are reduced with an increase in ΔZ. The stress σ_z on the sample during operation of piezo-response mode can be estimated according to $\sigma_z = F/\pi r^2$, where F is the force in Fig. 3(b) and r is the radius of the 35 nm curvature of the tip. The maximum value of repulsive σ_z that we obtained is 47 MPa. When the stress changes from repulsive 47 MPa to zero, then to attractive 60 MPa, the PEI signals are reduced by ~24% for positive poling areas, and by ~16% for negative poling areas.

Figures 7(a)–7(c) schematically illustrate PEI images obtained under repulsive force, attractive force, and during breaking of a water bridge as the sample displacement increases. The PEI image in Fig. 5(b) at $\Delta Z = 0$ was obtained under repulsive force of about 180 nN [see Fig. 3(b)]. From curves C′–C–D–D′ in Fig. 3(b), it can be seen that the force on the surface of the sample is repulsive when the sample displacement is less than 120 nm, which is illustrated in Fig. 7(a). When sample displacement is increased from 120 nm, attractive force develops, as illustrated in Fig. 7(b). The tip is pulled down about 75 nm at the pull-off point, which produces maximum attractive force of 230 nN. Some dark lines occur at the end of scan lines in PEI images as a water bridge broke with the increase in sample displacements up to 185 and 205 nm [Figs. 5(c) and 5(d)], as illustrated in Fig. 7(c). $A\cos\theta$ signals significantly change at the moment a water bridge breaks, which can be explained by the parameters in Eq. (4). Returning the tip from the pull-off position to a balanced position causes a change of z of 75 nm. The electric capacitance C and the difference in potential V_C are also different in contact and noncontact modes.[5]

V. CONCLUSIONS

(1) An ac voltage between the tip and the PZT bottom electrode increases attractive and pull-off forces. The stay time before the change in direction of sample displacement also affects the position of pull-off force.
(2) PEI images are obtained if the tip touches the sample. Whole PEI images can be formed under either repulsive or attractive force between the tip and the sample. PEI images are partially obtained when the tip separates from the sample during scanning. The PEI image disappears as the tip is disconnected from the sample.
(3) $A\cos\theta$ signals in positive and negative poling areas are asymmetrical under repulsive force and nearly symmetrical under attractive force. When stress on the film changes from repulsive 47 to attractive 60 MPa, the PEI signals are reduced by about 28% for positive poling areas, and by 16% for negative poling areas.

ACKNOWLEDGMENT

This work was funded by the Hong Kong Polytechnic University through Research Grant No. G-YW86.

[1] C. H. Ahn, T. Tybell, L. Antognazza, K. Char, R. H. Hammond, M. R. Beasley, O. Fisher, and J. M. Triscone, Science **276**, 1100 (1997).
[2] L. Jie, C. Baur, B. Koslowshi, and K. Dransfeld, Physica B **204**, 318 (1995).
[3] J. A. Christman, R. R. Woolcott, Jr., A. I. Kingon, and R. J. Nemanich, Appl. Phys. Lett. **73**, 3851 (1998).
[4] T. Hiddaka *et al.*, Appl. Phys. Lett. **68**, 2358 (1996).
[5] S. Hong, J. Woo, H. Shin, J. U. Jeon, Y. E. Pak, E. L. Colla, N. Setter, E. Kim, and K. No, J. Appl. Phys. **89**, 1377 (2001).
[6] G. Zavala, J. H. Fendler, and S. Trolier-McKinstry, J. Appl. Phys. **81**, 7480 (1997).
[7] G. D. Hu, J. B. Xu, and I. H. Wilson, Appl. Phys. Lett. **75**, 1610 (1999).
[8] A. Gruveman, H. Tokumoto, A. S. Prakash, S. Aggarwal, B. Yang, M. Wuttig, R. Ramesh, O. Auciello, and T. Venkatesan, Appl. Phys. Lett. **71**, 3492 (1997).
[9] T. Hidaka, T. Maruyama, M. Saitoh, and N. Mikoshiba, Appl. Phys. Lett. **68**, 2358 (1996).
[10] C. Loppacher, F. Schlaphof, S. Schneider, U. Zerwech, S. Grafstrom, L. M. Eng, A. Roelofs, and R. Waser, Surf. Sci. **532**, 482 (2003).
[11] R. Levy and M. Maaloum, Nanotechnology **13**, 33 (2002).
[12] R. Wiesendanger, *Scanning Probe Microscopy and Spectroscopy—Methods and Application* (Cambridge University Press, Cambridge, 1994), pp. 238–239.
[13] M. Salmeron, L. Xu, J. Hu, and Q. Dai, MRS Bull. **22**, 36 (1997).
[14] S. D. Campbell and A. C. Hillier, Langmuir **15**, 891 (1999).
[15] B. Cappella and G. Dietler, Surf. Sci. Rep. **34**, 1 (1999).
[16] J. F. Li, D. Viehland, C. D. E. Lakeman, and D. A. Payne, J. Mater. Res. **10**, 1435 (1996).
[17] A. L. Kholkin, E. L. Colla, A. K. Tagantsev, D. V. Taylor, and N. Setter, Appl. Phys. Lett. **68**, 2577 (1996).

Downloaded 18 Mar 2011 to 158.132.161.9. Redistribution subject to AIP license or copyright; see http://jap.aip.org/about/rights_and_permissions